

PAPER • OPEN ACCESS

Substrate critical effect on the structural and H₂ Gas sensing characteristics of solution-processed Zn_{0.075}Cu_{0.025}O films

To cite this article: Fatma Sarf *et al* 2021 *Mater. Res. Express* **8** 126401

View the [article online](#) for updates and enhancements.

You may also like

- [Griffiths phase, magnetic memory and ac susceptibility of an antiferromagnetic titanate-based perovskite Er_{0.9}Sr_{0.1}Ti_{0.975}Cr_{0.025}O₃ system](#)
R Hamdi, M Smari, A Bajorek *et al.*
- [Improvement of the low-field-induced magnetocaloric effect in EuTiO₃ compounds](#)
Shuang Zeng, , Wen-Hao Jiang *et al.*
- [Review—High-Capacity Li\[Ni_{1-x}Co_xMn_{1-x}\]O₂ \(x = 0.1, 0.05, 0\) Cathodes for Next-Generation Li-Ion Battery](#)
Chong S. Yoon, Moon Ho Choi, Byung-Beom Lim *et al.*



ECS Membership = Connection

ECS membership connects you to the electrochemical community:

- Facilitate your research and discovery through ECS meetings which convene scientists from around the world;
- Access professional support through your lifetime career;
- Open up mentorship opportunities across the stages of your career;
- Build relationships that nurture partnership, teamwork—and success!

Join ECS!

Visit electrochem.org/join





PAPER

Substrate critical effect on the structural and H₂ Gas sensing characteristics of solution-processed Zn_{0.075}Cu_{0.025}O films

OPEN ACCESS

RECEIVED

21 October 2021

REVISED

22 November 2021

ACCEPTED FOR PUBLICATION

1 December 2021

PUBLISHED

10 December 2021

Original content from this work may be used under the terms of the [Creative Commons Attribution 4.0 licence](#).

Any further distribution of this work must maintain attribution to the author(s) and the title of the work, journal citation and DOI.

Fatma Sarf¹, Irmak Karaduman Er² , Emin Yakar³ and Selim Acar⁴¹ Department of Management and Organization, Çan Vocational School, Çanakkale Onsekiz Mart University, Çanakkale, Turkey² Department of Medical Services and Techniques, Eldivan Medical Services Vocational School, Çankırı Karatekin University, Çankırı, Turkey³ Department of Materials Science and Engineering, Engineering Faculty, Çanakkale Onsekiz Mart University, Çanakkale, Turkey⁴ Department of Physics, Faculty of Science, Gazi University, Ankara, TurkeyE-mail: irmakkaradumaner@karatekin.edu.tr**Keywords:** metal oxides, chemical bath deposition, H₂ gas sensing, resistive sensor**Abstract**

In this study, we report the synthesis of Zn_{0.075}Cu_{0.025}O films by chemical bath deposition to determine the effect of substrate (glass slide or ZnO seed layer) on the structural and H₂ gas sensing properties of the produced films. The crystal phase, structural topography, surface morphology, and functional groups of the as-synthesized films as well as H₂ gas sensing properties were investigated. Although both films have a hexagonal wurtzite structure, ZnO seed layer-based Zn_{0.075}Cu_{0.025}O film is more crystalline than glass slide-based Zn_{0.075}Cu_{0.025}O films. ZnO seed layer-based Zn_{0.075}Cu_{0.025}O films exhibited much more nanorod and fewer nanosphere forms compared to glass slide-based Zn_{0.075}Cu_{0.025}O films. EDX analysis and Raman spectra of both samples confirmed the presence of defects in Cu: ZnO samples. ZnO seed layer-based sensors showed higher response (140%) and lower operating temperature (80 °C) compared to glass slide-based sensors (87% response and 140 °C operating temperature). The most important thing to note here is that the fabricated sensors exhibited a high response at room temperature. The responses at room temperature were found as 46% and 23% for the ZnO seed layer-based and glass slide-based sensors, respectively. Sensors operating at room temperature are especially important for commercial applications.

1. Introduction

Although H₂ is a non-toxic gas, some of the hazards associated with hydrogen usage can be given as follows; respiratory distress and suffocation, phase changes, component failures, ignition, and combustion. In most cases, a combination of these dangers can also occur. Precautions must be taken because the primary risk associated with any form of hydrogen is the possible fire or explosion by accidentally producing a flammable or detonable mixture [1]. Therefore, fuel cell, battery and electrochemical research laboratories, oil and gas refining, manufacturing processes that use or generate hydrogen as well as oil and gas refining factories must use real-time, selective, and sensitive H₂ gas sensors. Previous studies involving H₂ gas sensors have been carried out using various metal oxides such as SnO₂, ZnO, and NiO. Among them, ZnO material has been widely employed to detect a series of inorganic gases and organic vapors due to 3.37 eV wide bandgap energy, 60 meV binding energy, good chemical stability at high temperature, and high electron mobility [2]. Researchers have extensively used ZnO material for gas sensing applications because of matching good sensor performance [3]. It is primarily aimed to improve the gas detection properties of ZnO material by using different strategies. Zhou *et al* have prepared a ZnO sensor and investigated its NO₂ gas sensing performances under UV-activated sensing performance at room temperature (25 °C) [4]. Wang *et al* have studied a NO₂ sensor featuring composite film of few-layer black phosphorus (BP) nanosheets and zinc oxide nanowires serving as the sensing layer. BP-ZnO sensor exhibited 74% sensing performance compared to undoped one (37.7% for 50 ppb NO₂ gas) [5]. Zhou *et al* have studied cuprous oxide grown onto reduced graphene oxide nanosheets prepared to serve as the sensing

layer. Compared to the partial recovery at 25 °C, the sensor showed a response of 20% toward 1 ppm H₂S at 40 °C [6].

Creating new active centers on the surface or altering the surface/volume ratio of materials are the main strategies of these studies to decrease operating temperatures and detectable threshold of H₂ gas concentration down to low ppm levels [7]. With the use of dopant materials, the control of impurities in wide bandgap semiconductors can lead to surprising changes in the charge carrier properties [8]. Therefore, the doping process with metals of compatible ionic radius and high electrical conductivity is often preferred. Copper is a proper dopant metal for ZnO semiconductor due to its high electrical conductivity ($58.7 \times 10^6 \text{ S m}^{-1}$), similar ionic radius ($r_{\text{Cu}^{2+}} = 0.72 \text{ \AA}$ and $r_{\text{Zn}^{2+}} = 0.74 \text{ \AA}$) and tendency of altering oxygen vacancies with Cu²⁺ doping.

Researches on the operation of Cu:ZnO films as a gas sensor in recent years can be given as follows; Brahma *et al* have investigated room temperature acetone sensors using Cu:ZnO thin films [9]. Alev *et al* have reported that 3% Cu-doped ZnO nanorods showed the highest sensor response to ethanol which is 5.5 times higher than that of pure ZnO with increased surface oxygen species and lowered activation energy by Cu doping [10]. When Zn_{0.90}Cu_{0.10}O samples were investigated for the detection of NO gas, improved sensing performance was observed at an operating temperature of 55 °C as was shown in our previous study [11]. By sol-gel process used with different types of precursors, Gómez-Pozos *et al* have reported that the maximum sensitivity was exhibited in Cu-doped ZnO films prepared using copper chloride and deposited with eight immersions [12]. Bearing that H₂S production is usually accompanied by H₂, Shewale *et al* have shown that the selective performance was good in Cu:ZnO/rGO structures that exhibited high sensitivity towards H₂S gas [13]. ZnO seed layer acts as a nucleation center and so it provides a more stable structure and larger nucleation sites. Therefore, particle growth can be controlled with an easy coating on ZnO seed layer. In addition, using ZnO seed layer can reduce the lattice mismatch between the growing layer and substrate [14]. Gonzalez-Garnica *et al* have shown that ZnO nanowires with seed layers have much more sensitivity towards CO₂ gas [15]. In the present work, a systematic study was carried out to determine the possible effects of the type of substrate on the structural, morphological, and H₂ gas sensing properties of Zn_{0.075}Cu_{0.025}O films synthesized by chemical bath deposition.

2. Experimental

Firstly, the used microscope glasses were cleaned in an ultrasonic mixer with ethanol, then acetone and finally pure water and dried at room temperature. The cleaned glasses were kept in the conditioned solution for 15 min to allow ZnO to adhere to the glass surface more easily. The ratio of ammonia (NH₃)/trimethylamine (TEA)/pure water in this conditioning solution was set as 4:2:25. As a zinc (Zn) solution source, 99.99% purity Zn(CH₃COO)₂·2H₂O (zinc acetate dihydrate) was used. First, 0.1 M and 100 ml of zinc aqueous solution was prepared. 10 ml of ammonium hydroxide (NH₄OH) (26%) solution was added dropwise and the solution was mixed with a magnetic stirrer.

Ammonia was added to make the zinc source alkaline, and as ammonia was added, solution color changed from milky white to colorless, and the pH value of this solution was set to 10. Then, pure water was added to this solution until it reached 500 ml and a (NH₄)₂ZnO₂ bath was obtained. When the solution was examined the next day, it was observed that Zn(OH)₂ formed a white precipitate at the bottom. 20 ml of this prepared solution and 60 ml of distilled water were taken and the solution mixed in the beaker was placed on a magnetic stirrer at 50 ± 5 °C (pH 9.8). The films were taken from the conditioned solution, immersed in this mixture and left for 5 min. The films were left to dry for one day and then dried in an oven at 100 °C the next day; thus, weakly adherent structures were removed from the surface of the obtained ZnO seed layer.

After that, Cu-doped ZnO thin film was deposited on the synthesized ZnO seed layer. First, Zn(Ac)₂·2H₂O (Sigma Aldrich), copper powder (Sigma Aldrich) and NH₃ (Sigma Aldrich) were used as the source materials and complex agents. Initially, zinc source was dissolved in distilled water and stirred using magnetic stirrer. Copper source (at.% of 0.025) was added into the zinc-aqueous solution. Ammonia was added drop by drop to maintain the pH value at 10.4. The cleaned micro glass and ZnO seed layer [16] was used as substrates and they were immersed vertically with the help of a substrate holder. The solution was stirred by magnetic stirrer at 70 ± 5 °C in order to get the uniform coating on the substrate. After 20 min of deposition, the coated substrates were taken out from the solutions and cleaned with distilled water and was put on hold for a day. The coated substrates are kept in the furnace and annealed at 500 °C for 1 h.

The surface morphology and topography of the samples were analyzed using scanning electron microscopy (SEM, JEOL JSM-7100F) and atomic force microscopy (AFM, Witec alpha 300 RA) with non-contact mode. Elemental analysis was determined by energy dispersive x-ray spectrometer (OXFORD Instruments X-Max) attached to SEM. X-ray diffraction (XRD, Rigaku SmartLab) patterns of the samples were identified in the 2θ range of 20°–80° using CuK_α radiation ($\lambda = 1.5406 \text{ \AA}$), whilst Raman spectrum (Termo DXR) was employed to characterize the functional groups of the samples for 780 nm laser line. Gas measurements were taken in a fully

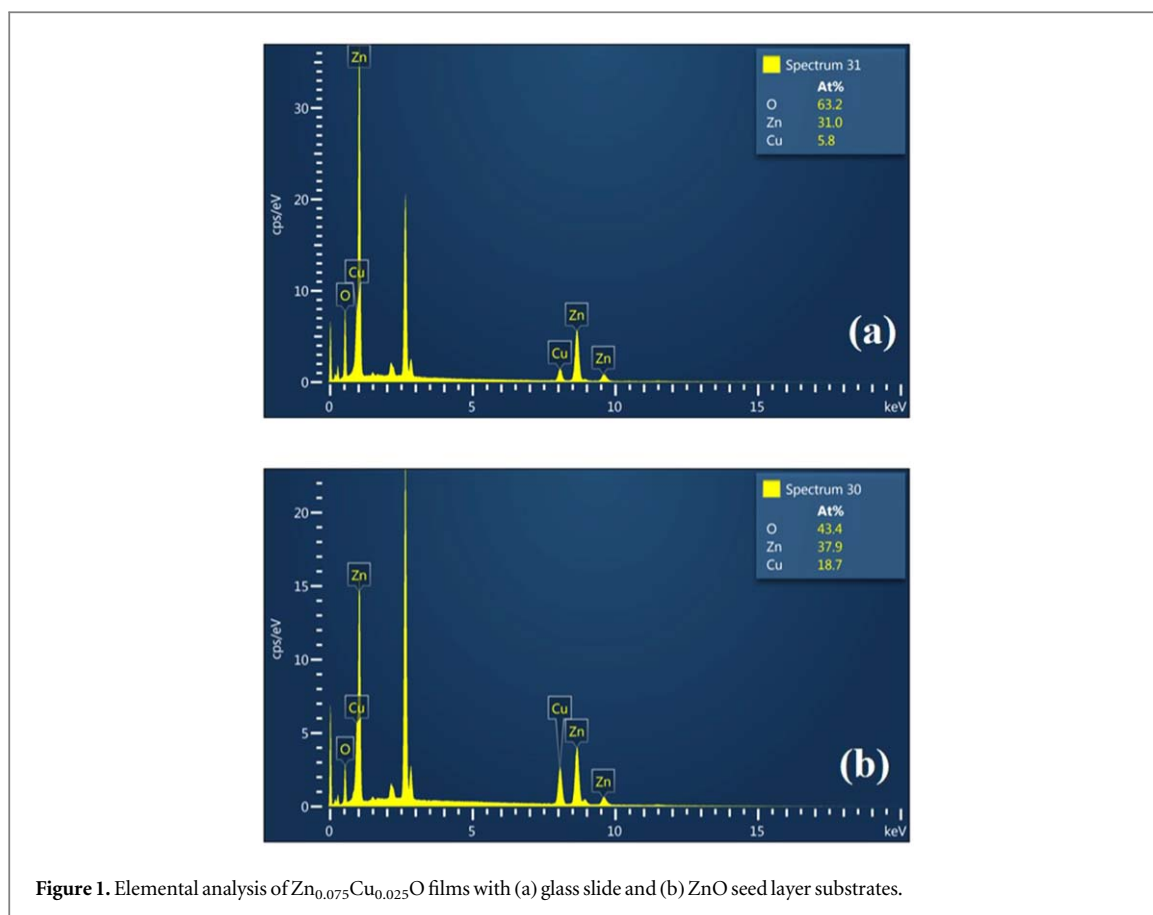


Figure 1. Elemental analysis of Zn_{0.075}Cu_{0.025}O films with (a) glass slide and (b) ZnO seed layer substrates.

computer-controlled gas detection system. The sensor cell consists of three parts: gas valves providing gas inlet and outlet, sample holder, and BNC connectors for necessary connections to Keithley 2400 device. Temperature-dependent measurements are made with the Lakeshore 325 temperature controller and gas measurements are made using the Keithley 2400 device. First, the sensors were fabricated and placed in the sensor cell. The sensor cell was then kept at a constant temperature using a temperature controller. With the help of gas flow controllers, target gas flow was provided to the sensor surface and measurements were taken. The flow rate of dry air entering the test cell was fixed at $500 \text{ cm}^3 \text{ min}^{-1}$ during the measurements. Air flow rate was kept constant under the same conditions in order to observe the behavior of different target gas concentrations. Sensor response degraded with humidity, in as much as water molecules and target gas compete in adsorption on the sensing surface which then leads to a decrease in sensitivity [17, 18]. Therefore, in this study, the humidity rate was kept constant at 25% to eliminate such effects.

The sensor response (S) was calculated using the following equation [19];

$$S(\%) = \left(\frac{R_g - R_a}{R_a} \right) \times 100 \quad (1)$$

where R_a is the resistance in dry air and R_g is the resistance upon exposure to the target gas. Response and recovery times are defined as the time interval when the resistance reaches 90% of the total change upon sending the target gas into the sensor cell and upon evacuating the target gas from the sensor cell, respectively [20].

3. Results and discussion

3.1. Elemental analysis

In figure 1, elemental analysis results of the samples are shown. The presence of atomic percentage (at.%) of Zn, O and Cu has been confirmed, which implies the formation of Cu:ZnO system. It is seen that the atomic percentage of copper in the structure is higher with the seed layer usage. It underlines that the atomic ratio of Zn/O for all samples, along with any other defects in the samples, as well as the presence of defects caused by oxygen vacancies in the samples, is the atomic ratio of Zn/O for all samples [21].

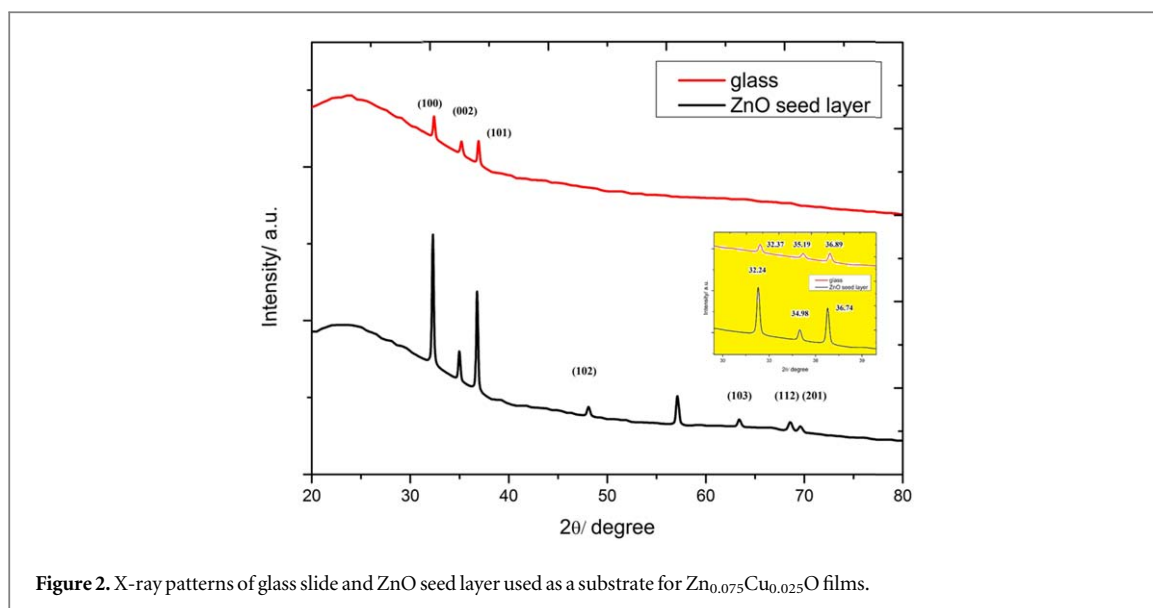


Figure 2. X-ray patterns of glass slide and ZnO seed layer used as a substrate for $\text{Zn}_{0.075}\text{Cu}_{0.025}\text{O}$ films.

Table 1. XRD parameters of glass slide and ZnO seed layer used as a substrate for $\text{Zn}_{0.075}\text{Cu}_{0.025}\text{O}$ films.

	2θ	d-spacing	FWHM	Crystallite size 'D' (nm)	Dislocation density δ ($\times 10^{-5} \text{ nm}^{-2}$)	Microstrain ϵ ($\times 10^{-2} \text{ line}^{-2} \text{ m}^{-4}$)
ZnO seed layer	(32.24)	2.7744	0.2312	69	14.5	5.52
	(34.98)	2.5629	0.2241			
	(36.74)	2.4432	0.2853			
Glass substrate	(32.37)	2.5331	0.3341	48	43.4	8.02
	(35.19)	2.3389	0.2491			
	(36.89)	2.3403	0.1611			

3.2. Structural characterization

X-ray patterns of the samples are illustrated in figure 2. All the patterns of both samples correspond to hexagonal wurtzite phase of ZnO with JCPDS card (36–1451). No secondary phase was observed in the samples due to the fact that Cu doping ratio was quite low and so copper cluster peaks were not detected. Similar copper doping optimization was realized by Roguai *et al* [22]. Copper doping ratio arrangement is important because initiation of copper doping can lead to an increase in the free energy of the system and a decrease in structural stability [23]. On the other hand, by introducing new phases above a certain doping ratio, the doping process can be eliminated, as explained by Sayed *et al* [24]. In the films where glass slide was used as a substrate, the x-ray diffraction intensities and FWHM remain quite weak compared to the films with ZnO seed layer substrate. The higher diffraction intensities of the ZnO seed layer-based samples means that the $\text{Zn}_{0.075}\text{Cu}_{0.025}\text{O}/\text{ZnO}$ layer film has an excellent crystal quality [25]. In addition, peaks other than the characteristic peaks in the range 30° – 40° could not be seen in the glass slide-based samples because there is a mismatch between the glass slide and the coated Cu:ZnO layer. This suggests that the ZnO seed layer is more ideal for film coating because it allows ZnO crystal growth with Cu doping, although it is intended for nanorod or nanowire growth [26, 27]. The slight shift in the original ZnO peaks' positions demonstrates that doping is successful by replacing the Zn^{2+} ions with Cu^{2+} ions in both of the samples. Table 1 gives the structural parameters of the samples.

For the hexagonal wurtzite, the lattice parameters (a and c) are computed by [28];

$$\frac{1}{d^2} = \frac{4}{3} \left(\frac{h^2 + hk + l^2}{a^2} \right) + \frac{l^2}{c^2} \quad (2)$$

The calculated lattice constants are given in table 1. The c/a ratio is 1.633 in a stoichiometric wurtzite structure [29]. As seen, c/a ratio of all samples (table 2) is smaller than ideal which might be linked to the presence of oxygen vacancies V_{O} and extended defects [30]. The average crystallite sizes of the films were estimated using Debye Scherrer's formula, also the microstrain and dislocation density was computed by below equations [31–33];

$$D = \frac{0.94\lambda}{\beta \cos \theta} \quad (3)$$

Table 2. XRD parameters of glass slide and ZnO seed layer used as substrate for Zn_{0.075}Cu_{0.025}O films (continued).

	Lattice parameters		Aspect ratio 'c/a'	Bond length 'L' (Å)	APF	Volume of the nanoparticles	Volume of unit cell 'V' (Å) ³	No. of unit cells
	'a = b' (Å)	'c' (Å)						
ZnO seed layer	3.2023	5.1636	1.6124	1.9667	0.75	171919	45.85	3749
Glass substrate	3.1903	5.1441	1.6124	1.9595	0.75	57876	45.34	1262

$$\varepsilon = \frac{\beta \cos \theta}{4} \quad (4)$$

$$\delta = \frac{1}{D^2} \quad (5)$$

The dislocation density is a measure of the number of dislocations in a unit volume of crystalline material. One of the main parameters for determining crystallinity and its enhancement is dislocation density. It refers to the displacement of atoms relative to the reference lattice positions, and this can be associated with the heat generation and lattice vibration in the molecular bond. If the structure has a small dislocation density, its crystalline structure is better than the other ones. However, a larger dislocation density implies a higher hardness [34]. When table 1 is examined, it is seen that ZnO seed layer-based film has smaller dislocation density and microstrain values. According to Deepa *et al*, the lower the lattice strain and defect density are, the more the carrier density and surface oxygen adsorption can happen [35].

Continuing with the XRD analysis, the parameters given in table 2 were calculated with the help of the following equations. Equations (5–8) were used to calculate the volume of the unit cell (ϑ), bond length (L), APF and “u” values, respectively [36–39];

$$\vartheta = \frac{\sqrt{3}}{2} a^2 c \quad (6)$$

$$L = \sqrt{\left(\frac{a^2}{3} + \left(\frac{1}{2} - u\right)^2 c^2\right)} \quad (7)$$

$$\text{APF} = \frac{2\pi a}{3\sqrt{3}c} \quad (8)$$

$$u = \frac{a^2}{3c^2} + 0.25 \quad (9)$$

‘u’ is a measure of the amount by which an atom is displaced with respect to the next atom along the c-axis. ‘u’ values were calculated as 0.3782 and 0.3786 for ZnO seed layer and glass slide used as substrate for Zn_{0.075}Cu_{0.025}O films, respectively. The standard hexagonal structure of ZnO has an APF value of 74 % [40], while our results were 75 %. The small difference can be related to the substitutional effect of Cu. The calculated Zn-O bonds were 1.9667 Å and 1.9595 Å for ZnO seed layer and glass slide used as substrate for Zn_{0.075}Cu_{0.025}O films, respectively. In the literature, the value of Zn-O bond was obtained as 1.95 Å and our results are almost close to 1.95 Å value. This result reveals that there are structural defects within our samples,

especially oxygen vacancies [30].

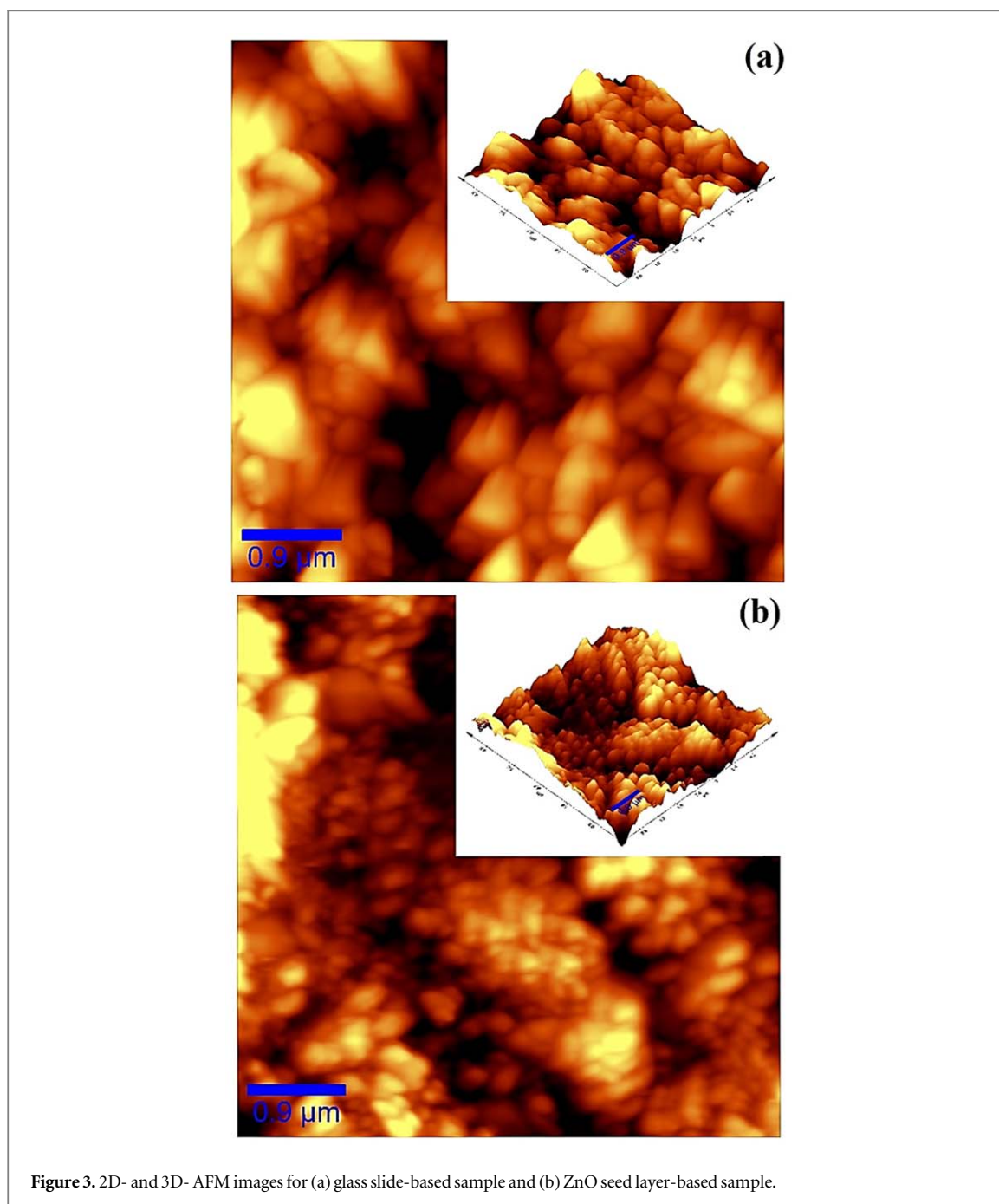
Then, the ratio (V/ϑ) gives the number of unit cells present in grain [41];

$$V = \left(\frac{4}{3}\right)\pi\left(\frac{D}{2}\right)^3 \quad (10)$$

All estimated structural parameters are consistent with the literature [41–45].

3.3. Surface morphology

To examine surface topography and surface roughness properties, figures 3(a) and (b) show the 2D- and (insets) 3D- AFM images of Cu:ZnO films deposited on the glass slide and ZnO seed layer substrates, respectively. When the 2D-AFM images were investigated, a clear and significant difference in the surface topography of both of the ZnO films was revealed depending on the used substrate type. The average roughness and rms values of the films increased with glass slide usage due to heterogeneous crystal growth and formation of large ZnO crystal forms. When SEM (figures 3(c) and (d)) and 3D-AFM images were examined together, it was observed that two nano-particle forming (granular and rod) appeared on the surface which affects the orientation of the particles in ZnO seed layer-based Zn_{0.075}Cu_{0.025}O films. In glass slide-based Zn_{0.075}Cu_{0.025}O films, the more irregular



distribution and random orientation of particles is noticeable although hexagonal particle formation is more pronounced. A similar study was conducted by Katı for Co:ZnO and explained that an increase in surface roughness has been observed due to a deterioration in the crystal structure, increase of defect intensities and deterioration in surface distribution [46]. As shown in figure 3, particle sizes decreased with ZnO seed layer usage. However, the very high average height values obtained by AFM analysis (431.4 and 128 nm) can be explained as follows, as elaborated by Farhad *et al*; the crystallite sizes obtained from XRD can be more accurate, since AFM analysis gives the crystallite size which can consist of more than one crystal and possible including of cluster forms [47].

The AFM analysis makes the synthesis of the samples repeatable and generalizes the results of the analysis from each part of the sample to the whole [48, 49]. Table 3 depicts some structural parameters from AFM analysis of Cu:ZnO films deposited on different substrates.

Under $\times 50,000$ magnification ratio, SEM images of the synthesized Cu:ZnO films are shown in figures 4(a) and (b). From these surface images, high density particle formations and no-crack forms were determined. Although there are granule structures of different sizes, the crystallite sizes of the granular forms are consistent with the results obtained from the Debye-Scherrer equation, which is measured for samples using glass substrates.

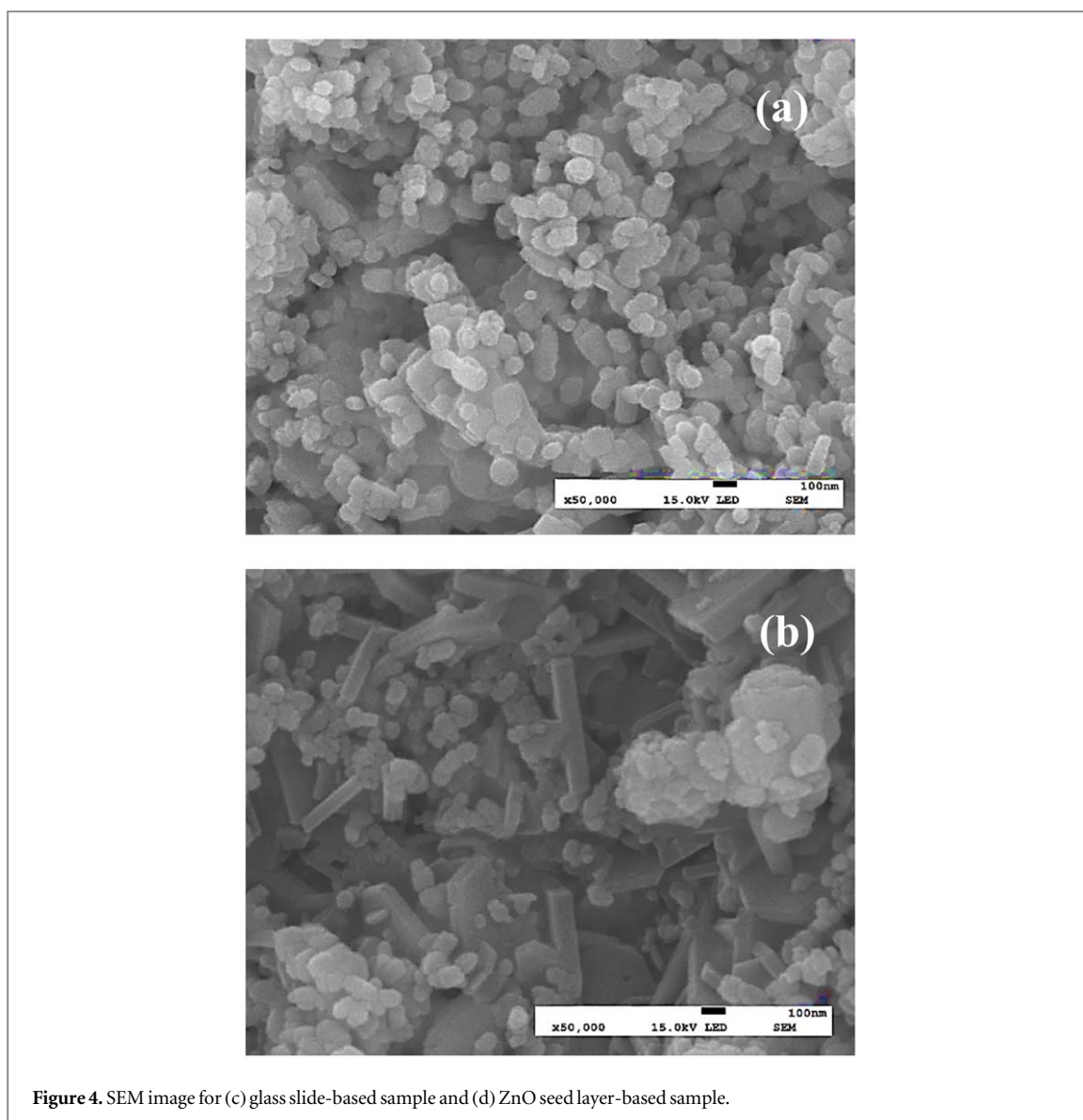


Figure 4. SEM image for (c) glass slide-based sample and (d) ZnO seed layer-based sample.

Table 3. The AFM analysis of Cu:ZnO films deposited on different substrates.

Substrate type	Root mean square, rms (nm)	Average roughness, Ra (nm)	Average Height (nm)
Glass slide	132.66	105.82	431.4
ZnO seed layer	48.88	40.70	128

Nanorod, decreasing nano-granular forms and big granular forms have been observed in ZnO seed layer-based samples. This morphological mixing and degradation by changing the substrate type to the ZnO seed layer can be explained by the increase in nucleation centers due to ZnO seed layer which can act as a nucleation center for Cu: ZnO crystal growth, as explained by Boukaous *et al* [50]. Increasing nanorod forms can be attributed to the lattice mismatch that might have occurred between the substrate and the coated Cu:ZnO layer [51].

3.4. Vibrational analysis

Figure 5 represents the Raman spectrum of the synthesized $\text{Zn}_{0.075}\text{Cu}_{0.025}\text{O}$ films in the spectral range between $250\text{--}1250\text{ cm}^{-1}$.

For a perfect ZnO crystal, optical phonon modes can be defined by the following description;

$$\Gamma_{\text{opt}} = A1 + E1 + 2E2 + 2B1$$

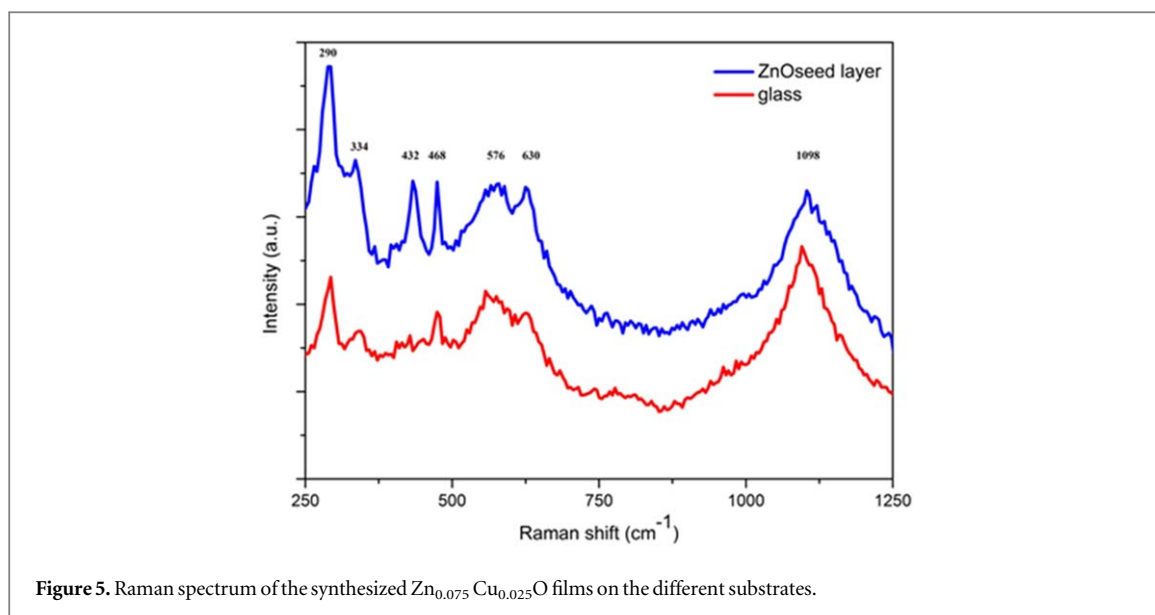


Figure 5. Raman spectrum of the synthesized $\text{Zn}_{0.075}\text{Cu}_{0.025}\text{O}$ films on the different substrates.

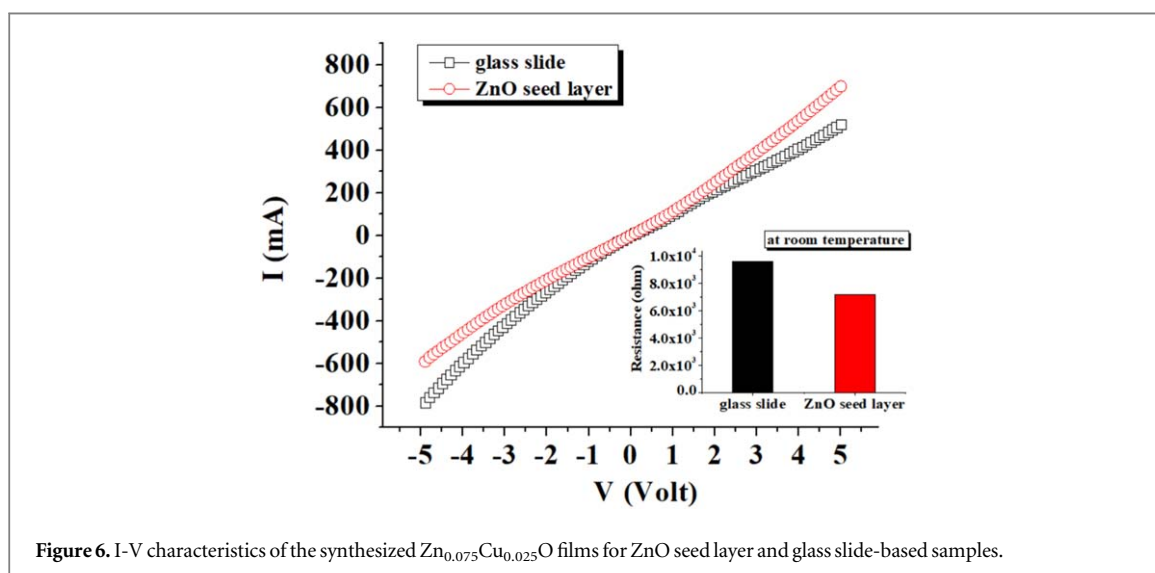
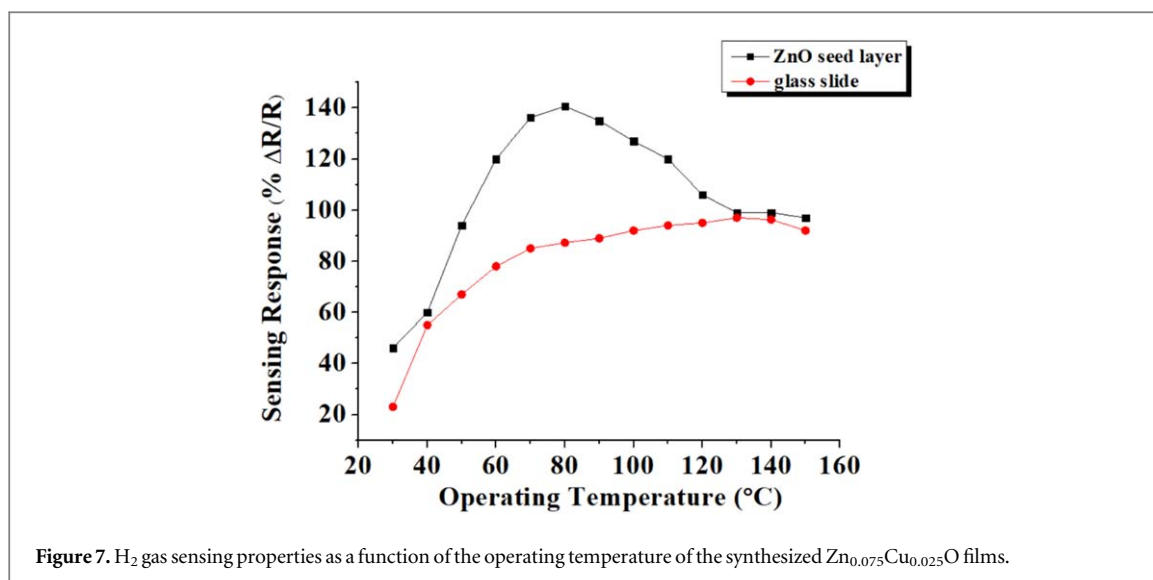


Figure 6. I-V characteristics of the synthesized $\text{Zn}_{0.075}\text{Cu}_{0.025}\text{O}$ films for ZnO seed layer and glass slide-based samples.

According to figure 5, seven typical vibrational peaks emerged in both samples at 290, 334, 432, 468, 576, 630 and 1098 cm^{-1} . The peak intensities of Raman modes of the films coated on ZnO seed layer are clearly higher than those of the films coated on glass slide. The peak at 334 cm^{-1} corresponds to optical phonon overtone with A1 symmetry [52]. The characteristic E2 (high) mode of wurtzite ZnO phase is observed at 432 cm^{-1} , especially in films coated on ZnO seed layer [21]. The presence of defects such as oxygen vacancies or interstitials zinc was manifested by peak of E1(TO) mode located at 468 cm^{-1} , indicating ZnO large crystal [53]. The peaks that are observed at 576 cm^{-1} and 630 cm^{-1} (Ribut *et al* have shown that these peaks were observed for ZnO/PET sample) can be assigned to A1(LO) phonon mode [24]. Abdelouhab *et al* reported that this peak was observed at 535 cm^{-1} , indicating that copper doping can cause a Raman shift due to ZnO phonon localization change by point defects and surface impurities [54]. Yin *et al* have shown that the vibration absorption peak at 576 cm^{-1} is closely related to the oxygen vacancies of ZnO [55]. The sharp peak observed at 1098 cm^{-1} corresponds to CH vibrations and is probably caused by indestructible aqueous solution [56]. In both samples, a slight shift from the original ZnO phonon mode locations were detected due to surface roughness and defects with copper doping effect. From Raman spectrum, E1(LO) phonon mode peak shift is in well agreement with EDX results to prove the presence of defects.

3.5. Electrical properties

Figure 6 depicts I-V characteristics of the synthesized $\text{Zn}_{0.075}\text{Cu}_{0.025}\text{O}$ films for ZnO seed layer- and glass slide-based samples at room temperature. Both samples exhibited the Ohmic behavior. The resistance of the samples



were calculated as 96.15 kΩ and 71.53 kΩ for glass slide- and ZnO seed layer-based samples, respectively. It can be inferred from other literature studies that the presence of ZnO seed layer increases current conduction and changes the current-voltage graphs [57–59].

3.6. H₂ gas sensing properties

To investigate the optimum operating temperature of the sensors, the gas chamber was subjected to an operating temperature from 30 °C to 150 °C and the gas response was calculated. Figure 7 shows the H₂ gas sensing properties (500 ppm) of the sensors as a function of operating temperature. The most notable thing is that both sensors exhibited high responses at room temperature. The responses at room temperature were found as 46% and 23% for the ZnO seed layer-based sensor and glass slide-based sensor, respectively. Sensors operating at room temperature are very important for commercial applications.

Mustafa *et al* have reported that they have grown ZnO thin films by magnetron sputtering technique and optimized their producing parameters. They obtained acceptable responses for hydrogen gas at room temperature [60]. Hassan *et al* have reported that ZnO nanorods were produced with the microwave-assisted chemical bath deposition method. They used Polyvinylalcohol (PVA)–Zn(OH)₂ nanocomposite as a seed layer and they have carried out the hydrogen gas sensing measurements at room temperature and reported that using a seed layer made the sensors work at low operating temperatures [61]. The optimal operating temperature was found at 80 °C and 140 °C for the ZnO seed layer-based sensor and glass slide-based sensor. After this temperature, responses began to decrease. The energy of the oxygen atoms sent to the surface increases with increasing temperature. However, after a certain critical temperature, the increase in energy values becomes too much, so that oxygen atoms can no longer hold onto the surface [62]. This causes instability and prevents the desired reaction with the target gas and thus, a decrease in sensitivities starts to be observed. Therefore, each sensor material has a unique operating temperature. In addition, the improved gas response of the Cu-doped ZnO samples might be due to the effects of the Cu ions on the ZnO surface properties, defects, and the large oxygen vacancy concentration [62].

The glass-based sample always has an uptrend but the ZnO seed-based sample has a maximum at 80 °C. This can be associated with the seed layer effect. ZnO structures were grown on different substrates and so the difference in trend can be attributed to the nature, surface topography and structure of substrates as well as the lattice mismatch with the synthesized nanostructures. These are particular significant parameters that can be factors to control the morphology and nature of the synthesized ZnO structures [63, 64].

The dynamic gas sensing measurements were carried out at 80 °C for both sensors, as shown in figure 8. The responses increased with increasing gas concentrations. The responses of the Zn_{0.075}Cu_{0.025}O films on the glass slide were calculated as 19%, 50%, 58%, 68%, 79% and 87% for 50 ppm, 100 ppm, 150 ppm, 200 ppm, 250 ppm and 500 ppm, respectively. It can be seen from the measurements that the sensors showed different responses for each gas concentration, the sensitivity increased with increasing gas concentration and the sensor resistance returned to its initial value when the gas entering the test cell was turned off. The responses of the Zn_{0.075}Cu_{0.025}O films on the ZnO seed layer were calculated as 58%, 68%, 79%, 85%, 99% and 140% for 50 ppm, 100 ppm, 150 ppm, 200 ppm, 250 ppm and 500 ppm, respectively. There is an exchange of electrons from

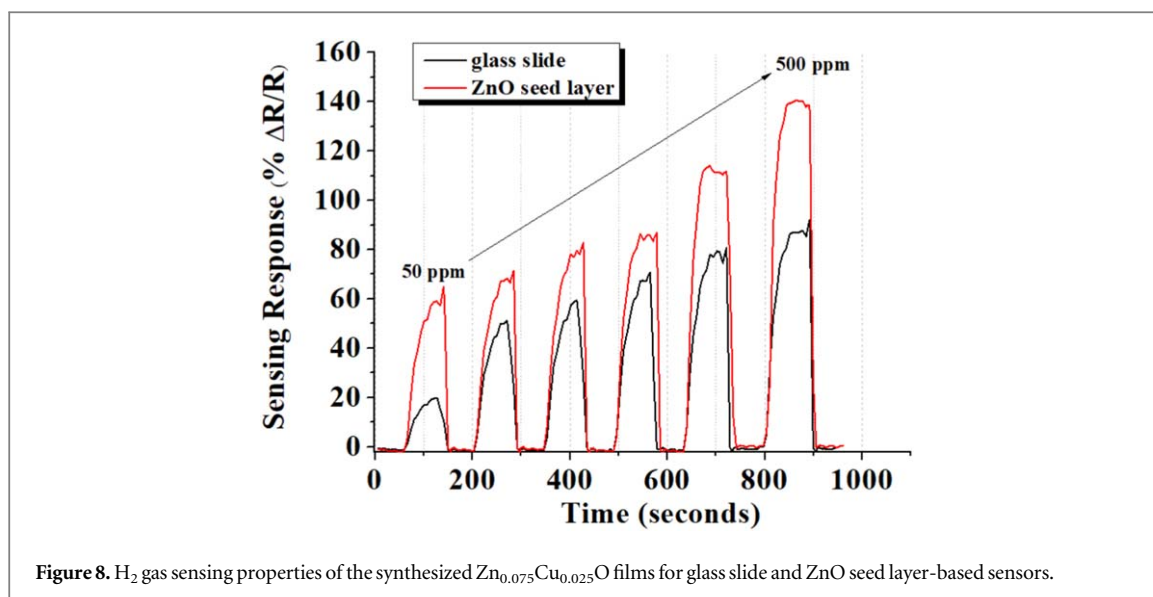


Figure 8. H_2 gas sensing properties of the synthesized $Zn_{0.075}Cu_{0.025}O$ films for glass slide and ZnO seed layer-based sensors.

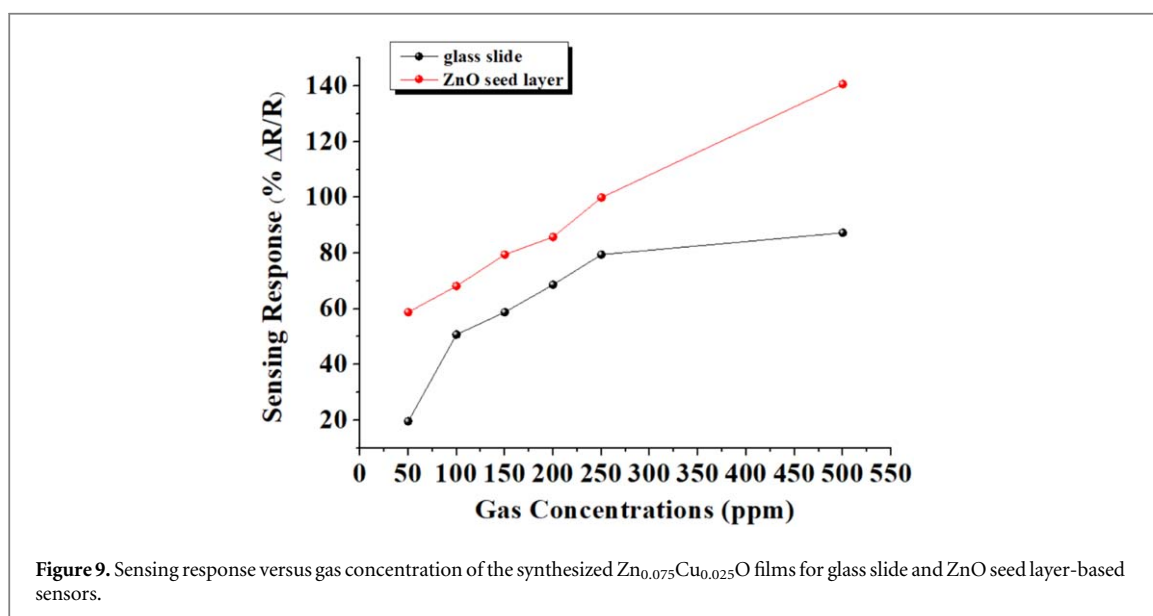


Figure 9. Sensing response versus gas concentration of the synthesized $Zn_{0.075}Cu_{0.025}O$ films for glass slide and ZnO seed layer-based sensors.

the lower ZnO seed layer to the upper layer, thus increasing the number of free electrons in the structure which results in an n-n heterostructure. Studies in this form are also available in the literature [61].

It is seen that higher gas responses were obtained in the sample grown on the ZnO seed layer. These results are consistent with the XRD analysis. Referring to table 1, the sample grown on the ZnO seed layer has a lower lattice strain and defect density which can lead to more carrier density and surface oxygen adsorption [35]. In addition, the volume of nanoparticles was higher for the ZnO seed layer-based sample, as shown in table 2. As the number of nanoparticles increases, the amount of gas adsorbed to the surface will increase.

Also, the doping process leads to increases in gas responses. When ZnO structure was doped with Cu, some of the Zn^{2+} ions in the ZnO structure get replaced by Cu^{2+} ions. As a result, Cu-Zn complex defects occur which may lead to more electrons in the conduction band [65]. The doping of Cu can occur more increasing charged oxygen vacancies because of the formation of more surface-absorbed oxygen [66]. With the increment of active adsorption regions, an increment in adsorbed gas molecules can be detected [9]. However, the distribution of Cu in ZnO thin films is not homogeneous, which may also help to form defects such as Cu interstitial and oxygen vacancies. Thus, the $Zn_{0.075}Cu_{0.025}O$ films on the ZnO seed layer and glass slide, can both of them generate oxygen vacancy defects easily with the Cu doping process. It can be found in the literature that Cu doping leads to corrections in the sensor parameters. Nimbalkar *et al* have reported that copper-doped zinc oxide thin films were successfully prepared by sol-gel spin coating technique and their H_2S gas sensing properties were investigated [67]. The Cu-doped ZnO thin film can stand as a prospective candidate for the detection of H_2S gas at low concentration (5–50 ppm). Chow *et al* have reported that Cu-ZnO sensors were produced by

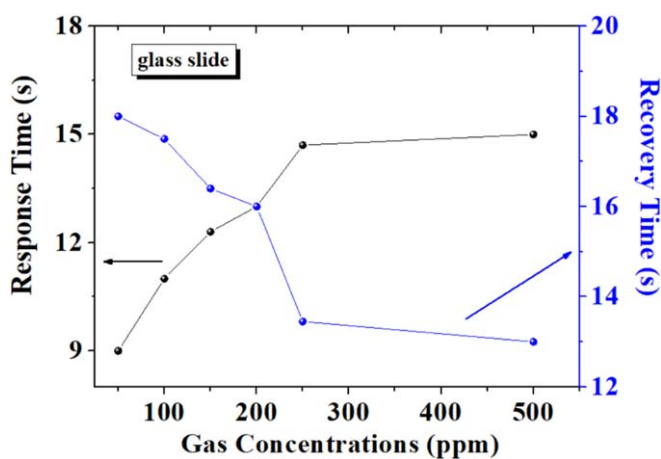


Figure 10. Response and recovery times versus gas concentration of the synthesized $Zn_{0.075}Cu_{0.025}O$ films for glass slide.

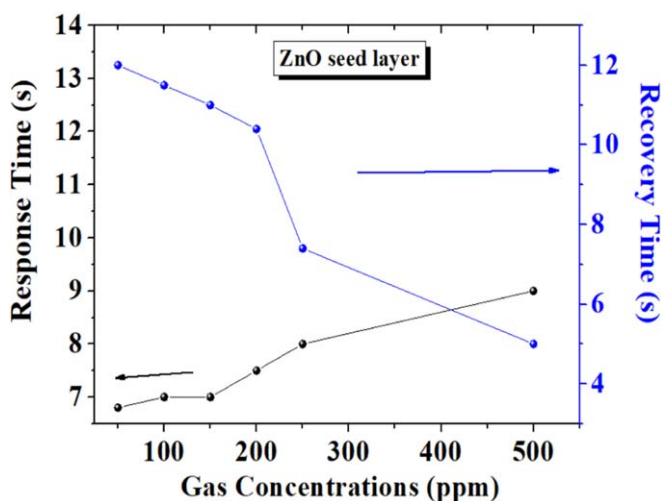


Figure 11. Response and recovery times versus gas concentration of the synthesized $Zn_{0.075}Cu_{0.025}O$ films for ZnO seed layer.

hydrothermal synthesis method. They have found that Cu-ZnO sensors showed room-temperature sensitivity to H_2 gas with low power consumption [68]. Figure 9 depicts the gas responses versus gas concentrations at $80^\circ C$ where almost a linear increase was observed for both sensors.

Response and recovery times are other important parameters for gas sensors. Figures 10 and 11 give the response and recovery times of both sensors where measurements were taken at the optimum operating temperature. Based on the obtained results, it has been seen that the thin films produced can be used as sensor materials in commercial applications. The response and recovery times for 50 ppm H_2 gas were found respectively as 7 s and 12 s for ZnO seed layer-based sensor as well as 9 s and 18 s for glass slide-based sensor. Apart from the sensor responses, both sensors have very fast response and recovery times.

Tables 4 and 5 give the H_2 gas sensing analysis of the synthesized $Zn_{0.075}Cu_{0.025}O$ films for ZnO seed layer and glass slide-based sensors, respectively. As can be seen from the tables, the sensors have very high responses at low operating temperature. In addition, the sensors have response and recovery times in the order of seconds. Based on these results, it can be said that the produced sensors can be used commercially easily.

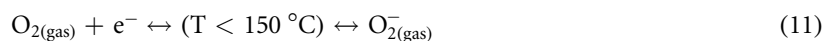
Generally, the gas sensing mechanism is a chemical reaction-based detection system [69]. The gas sensing mechanism can occur as two main reactions on the MOS sensor surface. In the first reaction, oxygen molecules in the air are chemically adsorbed on the sensor surface and the oxygen molecules transfer electrons in the conduction band towards it [70]. As a result of this transfer, oxygen molecules easily attach to the sensor surface and form an electron consumption region on the surface [70]. The second reaction takes place between the target gas and the oxygen molecules chemically adsorbed to the surface. An interaction of H_2 gas with molecular oxygen can take place as given by the below equations [61];

Table 4. H₂ gas sensing analysis of the synthesized Zn_{0.075}Cu_{0.025}O films for ZnO seed layer.

	Operating Temperature (°C)	Gas Concentrations (ppm)	Sensing Response (% ΔR)	Response Time (second)	Recovery Time (second)
ZnO seed layer	80	50	19.58	6.8	12
		100	50.70	7	11.5
		150	58.73	7	11
		200	68.63	7.5	10.4
		250	79.44	8	7.4
		500	87.27	9	5

Table 5. H₂ gas sensing analysis of the synthesized Zn_{0.075}Cu_{0.025}O films for glass slide.

	Operating Temperature (°C)	Gas Concentrations (ppm)	Sensing Response (% ΔR)	Response Time (second)	Recovery Time (second)
Glass Substrate	140	50	58.73	9	18
		100	68.15	11	17.5
		150	79.44	12.3	16.4
		200	85.76	13	16
		250	99.91	14.7	13.45
		500	140.64	15	13



Meanwhile, from the sensor response study, it is concluded that the synthesized Zn_{0.075}Cu_{0.025}O films on the ZnO seed layer are more preferable, indicating that the ZnO seed layer has noticeable positive effect on the gas sensing performance of the synthesized films.

Also, the effect of crystallite size is one of the important factors for gas sensing applications. When interpreted together with the volume of nanoparticles value, it was observed that the sample with ZnO seed layer had higher responses. Rothschild *et al* have reported that the response values they found in their study changed in proportion to the crystallite size D. When almost all the electrons are trapped at the surface, the carrier concentration of the surface state density reaches a critical value that shows a condition of fully depleted grains [71]. Savu *et al* have studied that tin oxide films were grown by two different methods, RF magnetron sputtering and doctor blade techniques, respectively. Because of the lower initial resistance and bigger crystallite size, the doctor-bladed samples can be shown more good sensing performance [72].

4. Conclusion

In this work, a trend change in H₂ gas sensitivity has been revealed and discussed by substrate type (glass slide or ZnO seed layer) of Cu:ZnO films. X-ray patterns, EDX analysis and Raman spectrum of both samples confirm the incorporation of Cu into the ZnO host matrix and the presence of localized defects by Cu doping. The most notable thing is that both sensors exhibited high responses at room temperature. The responses at room temperature was found as 46% and 23% for the ZnO seed layer-based sensor and glass slide-based sensor, respectively. Sensors operating at room temperature are very important for commercial applications. Apart from the sensor responses, both sensors showed very fast response and recovery times, though the sensor based on ZnO seed layer was more preferable. This signifies that the ZnO seed layer can have noticeable positive effects on the gas sensing performance of the synthesized films.

Data availability statement

All data that support the findings of this study are included within the article (and any supplementary files).

ORCID iDs

Irmak Karaduman Er  <https://orcid.org/0000-0003-3786-3865>

References

- [1] Nojumi H, Dincer I and Naterer G F 2009 *International Journal of Hydrogen Energy* **34** 1363–9
- [2] Choi M S, Kim M Y, Mirzaei A, Kim H-S, Kim S-i, Baek S-H, Chun D W, Jin C and Lee K H 2021 *Applied Surface Science* **568** 150910
- [3] Yang D, Ramu A G, Lee Y, Kim S, Jeon H, Sathishkumar V E, Al-Mohaimed A M, Al-onazi WA, Saad Algarni T and Choi D 2021 *Journal of King Saud University – Science* **33** 101397
- [4] Zhou Y, Wang Y, Wang Y, Li X and Guo Y 2020 *Ceramics International* **46** 16056–61
- [5] Wang Y, Zhou Y, Ren H, Wang Y, Zhu X, Guo Y and Li X 2020 *Analytical Chemistry* **92** 11007–17
- [6] Zhou Y, Wang Y and Guo Y 2019 *Materials Letters* **254** 336–9
- [7] Khudiar A I and Oufi A M 2021 *Sens. Actuators B* **340** 129633
- [8] Ali G A, Emam-Ismael M, El-Hagary M, Shaaban E R, Moustafa S H, Amer M I and Shaban H 2021 *Optical Materials* **119** 111312
- [9] Brahma S, Yeh Y-W, Huang J-L and Liu C-P 2021 *Appl. Surf. Sci.* **564** 150351
- [10] Alev O, Ergün İ, Özdemir O, Çolakkerol Arslan L, Büyükköse S and Öztürk Z Z 2021 *Materials Science in Semiconductor Processing* **136** 106149
- [11] Çorlu T, Karaduman I, Galioglu S, Akata B, Yıldırım M A, Ateş A and Acar S 2018 *Materials Letters* **212** 292–5
- [12] Gómez-Pozos H, Arredondo E J L, Álvarez A M, Biswal R, Kudriavtsev Y, Pérez J V Lucero Casallas-Moreno Y L C and de la Luz Olvera Amador M 2016 *Materials* **9** 87
- [13] Shewale P S and Yun K-S 2020 *Journal of Alloys and Compounds* **837** 155527
- [14] Ho Kim K, Utashiro K, Abe Y and Kawamura M 2014 *Int. J. Electrochem. Sci.* **9** 2080–9
- [15] Gonzalez-Garnica M et al 2021 *Sens. Actuators B* **337** 129765
- [16] Özütk F and Demiri S 2017 *Dig. J. Nanomater. Biostruct.* **12** 309–17
- [17] Alfano B et al 2019 *Sensors. CNS 2018. Lecture Notes in Electrical Engineering* 539 (Berlin: Springer) Cham.)
- [18] Cheng I-K, Lin C-Y and Pan F-M 2021 *Applied Surface Science* **541** 148551
- [19] Yıldırım M A, Yıldırım S T, Çağırtekin A O, Karademir M, Karaduman Er I, Coşkun A, Ateş A, and Acar S 2019 *Journal of Materials Science: Materials in Electronics* **30** 12215–23
- [20] Fu X, Sjiào S, Dong N, Lian G, Zhao T, Lv S, Wang Q and Cui D 2018 *RSC Adv.* **8** 390
- [21] Raji R and Gopchandran K G 2017 *Mater. Res. Express* **4** 025002
- [22] Roguai S and Djelloul A 2020 *Applied Physics A* **126** 122
- [23] Ma Z, Ren F, Ming X, Long Y and Volinsky A A 2019 *Materials* **12** 196
- [24] El Sayed A M, Said G, Taha S, Ibrahim A and Yakuphanoglu F 2013 *Superlattices and Microstructures* **62** 47–58
- [25] Ributa S H, Che Abdullah C A and Yusoff M Z M 2019 *Results in Physics* **13** 102146
- [26] Castillo-Rodríguez J, Pereyra C J, Valente P, Seré A, Marotti R E, Hevia S A, Dalchiele E A, del Rio and Quero R 2020 *Journal of Solid State Electrochemistry* **24** 797–808
- [27] Özütk F and Yakar E 2018 *Journal Of Applied Spectroscopy* **85** 1–6
- [28] Astuti B, Zhafirah A, Carieta V A, Hamid N, Marwoto P, Nurbaiti S U, Ratnasari F D, Putra N M D and Aryanto D 2020 *Journal of Physics Conference Series* **1567** 022004
- [29] Beltran J J, Osorio J A, Barrero C A, Hanna C B and Punnoose A 2013 *Journal of Applied Physics* **113** 17C308
- [30] Bilgili Ö 2021 *J. Baun Inst. Sci. Technol.* **23** 50–64
- [31] Girija K G, Somasundaram K, Topkar A and Vatsa R K 2016 *Journal of Alloys and Compounds* **684** 15–20
- [32] Eşgin H, Çağlar Y and Çağlar M 2021 *Journal of Alloys and Compounds* **890** 161848
- [33] Al-Ariki S, Yahya N A A, A. Al-A'nsi S, Hj Jumali M H, Jannah A N and Abd-Shukor R 2021 *Scientific Reports* **11** 11948
- [34] Kumar Sen S, Mortuza A A, Manir M S, Pervez M F, Hossain S M A I, Alam Md S, Haque M A S, Matin M A and M A Hakim, A-u 2020 *Nano Express* **1** 020026
- [35] Deepa S, Prasanna Kumari K and Boben T 2017 *International Journal for Research in Applied Science & Engineering Technology (IJRASET)* **5** IIX 2017
- [36] Sathya M and Pushpanathan K 2018 *Appl. Surf. Sci.* **449** 346–57
- [37] Srinivasan G, Rajendra Kumar R T and Kumar J 2007 *J Sol-Gel Sci Technol* **43** 171
- [38] Thakur S, Sharma N, Varkia A and Kumar J 2014 *Advances in Applied Science Research* **5** 18–24
- [39] Bilgili Ö 2021 *J. Baun Inst. Sci. Technol.* **23** 50–64
- [40] Kebiroğlu H et al 2020 *Düzce University Journal of Science & Technology* **8** 1634–49
- [41] Mariappan R, Ponnuswamy V, Chandra Bose A, Chithambararaj A, Suresh R and Ragavendar M 2014 *Superlattices Microstruct* **65** 184–94
- [42] Goktas A 2018 *J. Alloys Compd.* **735** 2038–45
- [43] Manzoor M F et al 2019 *Acta Physica Polonica A* **135** 3
- [44] Wang X, Zheng R, Liu Z, Ho H-P, Xu J and Ringer S P 2008 *Nanotechnology* **19** 455702
- [45] Nurfani E, Kesuma W A P, Lailani A, Anrokhi M S, Kadja G T M, Rozana M, Sipahutar W S and Arif M F 2021 *Optical Materials* **114** 110973
- [46] Katı N 2019 *Turkish Journal of Science & Technology* **14** 41–8
- [47] Farhad S F U, Tanvir N I, Bashar N S, Hossain M S, Sultana M and Khatun N 2018 *Bangladesh J. Sci. Ind. Res.* **53** 233–44
- [48] Gharib M, Eshraghi M J and Bordbar M 2020 *J Mater Sci: Mater Electron* **31** 21515–27
- [49] Bhushan B 2000 *Modern Tribology Handbook, Two Volume Set* 1st ed. (Boca Raton, FL: CRC Press)
- [50] Boukaous C, Benhaoua B, Telia A and Ghanem S 2017 *Mater. Res. Express* **4** 105024
- [51] Elsayed K A, Anad N S, AbdelFattah G, Hisham Imam H, Kayed T S and Ismail L Z 2015 *Arabian Journal of Chemistry* **8** 553–9
- [52] Balan V, Mihai C-T, Cojocaru F-D, Uritu C-M, Dodi G, Botezat D and Gardikiotis I 2019 *Materials* **12** 2884
- [53] Song Y, Zhang S, Zhang C, Yang Y and Lv K 2019 *Crystals* **9** 395
- [54] Abdelouhab Z A, Djouadi D, Chelouche A and Touam T 2020 *Journal of Sol-Gel Science and Technology* **95** 136–45
- [55] Song Y, Lv K and Zhang S 2020 *Chinese Journal Of Materials Research* **34** 1

- [56] Dikmen G and Alver Ö 2021 *Eskişehir Technical University Journal Of Science And Technology A- Applied Sciences And Engineering* **22** 134–47
- [57] Somvanshi D and Jit S 2014 *IEEE Transactions On Nanotechnology* **13** 1138–44
- [58] Nandi R 2013 *AIP Conference Proceedings* **1512** 410
- [59] Novák P, Joe Briscoe J, Kozak T, Kormunda M, Netrvalová M and Bachratá S 2017 *Thin Solid Films* **634** 169–74
- [60] Mustafa S N A, Ariffin N A, Khalaf A L, Yaacob M H, Tamchek N, Paiman S and Sagadevan S 2020 *J. Mater. Res. Technol.* **9** 10624–34
- [61] Hassan J J, Mahdi M A, Chin C W, Abu-Hassan H and Hassan Z 2012 *Physica E* **46** 254–8
- [62] Sarf F, Karaduman E I, Yakar E and Acar S 2020 *Journal of Materials Science: Materials in Electronics* **31** 10084–95
- [63] Abdulrahman A F, Ahmed S M, Ahmed N M and Almessiere M A 2016 *Digest Journal of Nanomaterials and Biostructures* **11** 1007–16
- [64] Ahn H, Wikle III H C, Kim S-B, Liu D, Lee S, Park M and Kim D-J 2012 *Journal of The Electrochemical Society* **159** E23–9
- [65] Patil V L, Vanalakar S A, Tarwal N L, Patil A P, Dongale T D, Kim J H and Patil P S 2019 *Sensors and Actuators A* **299** 111611
- [66] Wang C, Zhu J, Liang S, Bi H, Han Q, Liu X and Wang X 2014 *J. Mater. Chem. A* **2** 18635–43
- [67] Nimbalkar A R and Patil M G 2017 *Materials Science in Semiconductor Processing* **71** 332–41
- [68] Chow L, Lupan O, Chai G, Khallaf H, Ono L K, Roldan Cuenya B, Tiginyanu I M, Ursaki V V, Sonte V and Schulte A 2013 *Sensors and Actuators A* **189** 399–408
- [69] Karaduman E I, Ali Yıldırım M A, Örkçü H H, Ateş A and Acar S 2021 *Applied Physics A* **127** 230
- [70] Altun B, Karaduman E I, Çağırtekin A O, Ajjaq A, Sarf F and Acar S 2021 *Applied Physics A* **127** 687
- [71] Rothschild A and Komem Y 2004 *Journal of Applied Physics* **95** 6374–80
- [72] Savu R, Ponce M A, Joanni E, Bueno P R, Castro M, Cilense M, Varela J A and Elson Longo E 2009 *Materials Research* **12** 83–7